Study on hot deformation behavior of beta Ti-17Mo alloy for biomedical applications

Saad Ebied [a, *], Atef Hamada [b], Mahmoud H.A. Gadelhaq [c], Kenta Yamanaka [d], Huakang Bian [d], Yujie Cui [d], Akihiko Chiba [d], Mohamed A.H. Gepreel [e]

[a] *Department of Production Engineering and Mechanical Design, Faculty of Engineering, Tanta University, Tanta, 31527, Egypt*
[b] *University of Oulu, Kerttu Saalsti Institute, Pajatie 5, Nivala FI-85500, Finland*
[c] *Department of Automotive Engineering, Faculty of Engineering, Ain Shams University, Cairo, Egypt*
[d] *Institute for Materials Research, Tohoku University,2-1-1 Katahira, Aoba-ku, Sendai 980-8577, Japan*
[e] *Egypt-Japan University of Science and Technology (E-JUST), New Borg El-Arab City, 21934, Alexandria, Egypt*

Abstract:

A novel biomaterial Ti-17Mo (mass %) was designed for orthopedic implant applications. Hot working behavior and deformation characteristics were studied in the β-single structure by hot compression tests in the strain rate range 0.01–10 s^{-1} and temperature range 1123–1273 °C using a Thermec Master-Z simulator. The microstructural evolutions of the deformed alloy are studied by a scanning electron microscope (SEM) equipped with an electron backscattered diffraction (EBSD) detector. The microstructures of the hot deformed alloy displayed that dynamic recovery was more active than dynamic recrystallization (DRX). However, partial discontinuous DRX by grain boundary bulging is activated at high temperatures and low strain rates, e.g., 1273 k and 0.01 s^{-1}. Due to the high stacking fault energy of the β phase with a bcc structure, the Ti-17Mo alloy possessed comparatively low activation energy of hot deformation (283 kJ/mol) compared with the conventional Ti alloys bearing multiple alloying elements.

Keywords: β- titanium alloys; hot deformation; deformation mechanism; activation energy; dynamic recovery; dynamic recrystallization.

Corresponding author:
E-mail: saad_ebied@f-eng.tanta.edu.eg (Saad Ebied)

1. Introduction

Titanium alloys are incorporated in various structural applications, such as biomedical, sports, aerospace, and automotive industries [1, 2]. It is well established that beta titanium alloys with a body-centered cubic (bcc) structure exhibit high specific strength, acceptable cold workability, moderate ductility and show excellent fatigue performance by increasing the Oxygen content [3]. Furthermore, β-Ti alloys show comparable mechanical properties to α-Ti alloys with a hexagonal close-packed (hcp) structure and α+β alloys, clarifying their high work hardening capacity [4]. The β-Ti alloys are heat-treatable alloys and uniform hard dispersion can be introduced using solution treatment in the beta field preceding subsequent aging at lower temperatures where the α and/or ω phases are stable. Furthermore, cold working is employed to alter the precipitation morphology in the metastable state to produce a high-level density of fine precipitates. Consequently, the mechanical and physical properties could be enhanced with deformation [5].

It is reported that Molybdenum (Mo) stabilizes the β phase in titanium alloys, hence adding the alloying element Mo to the Ti-based alloys promotes β-type structure [6]. Furthermore, Mo has low toxicity compared to V and Al. The Ti-15Mo alloy is a commercial Ti-Mo alloy and was evaluated for applications in orthopedic implants [7]. Last decade, Niinomi and his team at Tohoku University in Japan have developed a novel Ti-17Mo alloy with high biocompatibility and variable Young's modulus through cold working to induce ω phase to be implemented in spinal fixation equipment [8].

Understanding the metal deformation process at high temperatures is important because hot working is an important manufacturing process. Thermomechanical processing used for titanium alloys includes relatively complex forging steps. Generally, these alloys show a single bcc-β phase domain at high temperatures, while below a certain temperature nominated as transus temperature T_{β}, the material consists of hcp-α and bcc-β phase. The hot deformation of titanium alloys, specifically β and near-β Ti alloys, was reported in many previous publications, e.g., Refs. [8–10]. Several studies have reported that the dynamic recrystallization (DRX) mechanism is operated in β-Ti alloys in addition to the dynamic recovery (DRV) mechanism depending on the hot deformation parameters [11,12]. Particularly, DRV is generally preferred in β-Ti alloys because of their high stacking fault energy (SFE) [13,14].

In contrast, the DRX mechanism is complex and caused debates [8,15–17]. Some scientists suggested that discontinuous dynamic recrystallization (DDRX), which is ascribed to the nucleation process followed by the growth of new grains, work in these alloys over a bulging mechanism of the original grains [18]. In addition, continuous dynamic recrystallization (CDRX) occurs via a change process from low-angle grain boundaries (LAGBs) to high-angle grain boundaries (HAGBs) [19]. Recently, the continuous dynamic recrystallization (CDRX) mechanism has been proved to cause microstructure refinement and high hot formability in β-Ti alloys [20].

On the other hand, deformation bands (DBs) have been detected in some beta /Titanium alloys. Fan et al. [21] observed deformation bands (DBs) during the hot deformation of the Ti-5Al-5Mo-5V-3Cr-1Zr within the beta phase area. Kuhlmann et al. [22] reported that DB formation is mostly related to the selection method of the effective slip structures to reduce the consumption of energy during the deformation process, especially for coarse-grained material. Also, if the applied strain is distributed non-uniformly inside the deformed specimen the generation process of DB can be promoted [23]. The boundaries of the deformation bands are sharp, which are like the HAGBs. These sharp boundaries will hinder the recrystallization process.

Recently, Li et al. [24] studied enhancing the mechanical strength of Ti-Nb based alloy by adding Mo element at different atomic percent. They found that Mo addition stabilizes the alloys' β phase in addition to enhancing the strength without scarifying ductility. Moreover, the addition of Mo to Ti-Nb alloys induced anti-wear capacity, i.e., long shelf life as biomedical materials. Xu et al. [25] studied the Mo addition effect on corrosion and tribocorrosion behaviors of Ti-Mo alloys. They reported that with increasing Mo amount in the range of 8 - 20 (wt) %, the corrosion resistance of the studied Ti-Mo alloys is significantly increased. Fellah et al. [26] investigated the effect of Mo content on mechanical and wear resistance characteristics of binary Ti-Mo alloy. He reported that by increasing the Mo amount, both the mechanical properties and wear resistance increased.

It is noteworthy that one of the metallurgical bases for enhancing corrosion resistance and mechanical properties is grain refinement [27]. Also, there was not any reported study about hot deformation performed on Ti-Mo alloy with coarse structure till this research was conducted. In the present work, the deformation mechanisms in addition to the microstructural evolution throughout the hot deformation of Ti-17Mo alloy were investigated. Furthermore, the impact of the primary coarse structure on the hot deformation mechanism was studied.

It is very interesting to highlight that through this study of the new Ti-17Mo alloy, it would be possible to enhance the grain structure during the manufacturing of Ti-Mo alloys and thereby help to enhance mechanical properties concerning the strength and toughness compared with the conventional Ti alloys.

2. Experimental work

Ti-17 wt. % Mo alloy was produced by melting high purity Ti sponge and Mo in an electric arc furnace in an argon environment (ARCAST 200, USA) and cast into 100 gm ingots. Homogenization was done for the ingots at 1273 K for 28.8 ks under protective argon surrounding using quartz tube and muffle furnace. Then the ingots were hot deformed by rolling at 1123 K to 8.5 mm thick strips using a laboratory rolling mill. These strips were sealed in a quartz tube under an argon atmosphere and solution heat-treated at 1173 K for 1.8 ks min in a muffle furnace, followed by quenching in ice water by breaking the quartz tube immediately to obtain a complete β-phase structure at ambient conditions. Electrical discharge machining (EDM) was used to cut bars of 7.5 mm in diameter from the rolled strips. Subsequently, specimens in the cylindrical shapes of 6 mm in diameter and 9 mm in length were cut for hot compression testing so the compression axis is parallel to the rolling direction.

The hot deformation behavior of the β Ti-17Mo alloy was investigated via isothermal constant true strain rate compression tests using hot deformation simulator (Thermic Master-Z). Tested specimens were heated in a vacuum atmosphere (<1.0 Pa) at the rate of 10 K/s to the deformation temperature ranging from 1123 K to 1273 K with an interval of 50 K. Temperature was then held for 120 seconds to obtain a homogeneous temperature distribution through the sample. To lower the friction and increase the deformation homogeneity, a carbon sheet was put between the sample's surfaces and anvils. To reduce the heat dissipation, a mics sheet was put between the sample's surfaces and anvils. Then, the specimens were compressed to a true strain of 0.6 with a strain rate range of 0.01-10 s^{-1}. At end of the hot deformation straining, the deformed specimens were fast cooling by blowing a gaseous mixture of Ar and He to freeze the high-temperature deformation microstructure. The microstructure observation was carried out using electron backscatter diffraction (EBSD) on an FE-SEM (FEI, XL30S-FEG) at an operating voltage of 15 kV with a step size of 1 µm. The phase constituent of the solution treated Ti-17Mo was investigated via X-ray diffraction (XRD) analysis.

3. Results and discussions

3.1. Original microstructure

A fully β-bcc structure is promoted in the studied Ti-17Mo alloy after solution treatment at 1173 K, as shown in the inverse pole figure (IPF) map in

Fig. 1(a). However, the microstructure was relatively inhomogeneous, representing a bimodal grain size distribution an average grain size of 401 µm, as measured by EBSD. The X-ray profile of the solution-treated Ti-17Mo alloy, shown in

Fig. 1(b), confirms the fully β-bcc structure of the solution-treated alloy. Since all Bragg peaks in the XRD pattern were indexed for the β-bcc structure. It is worth mentioning here that the 17 wt.% Mo is sufficient to preserve fully β-phase structure at ambient conditions [28].

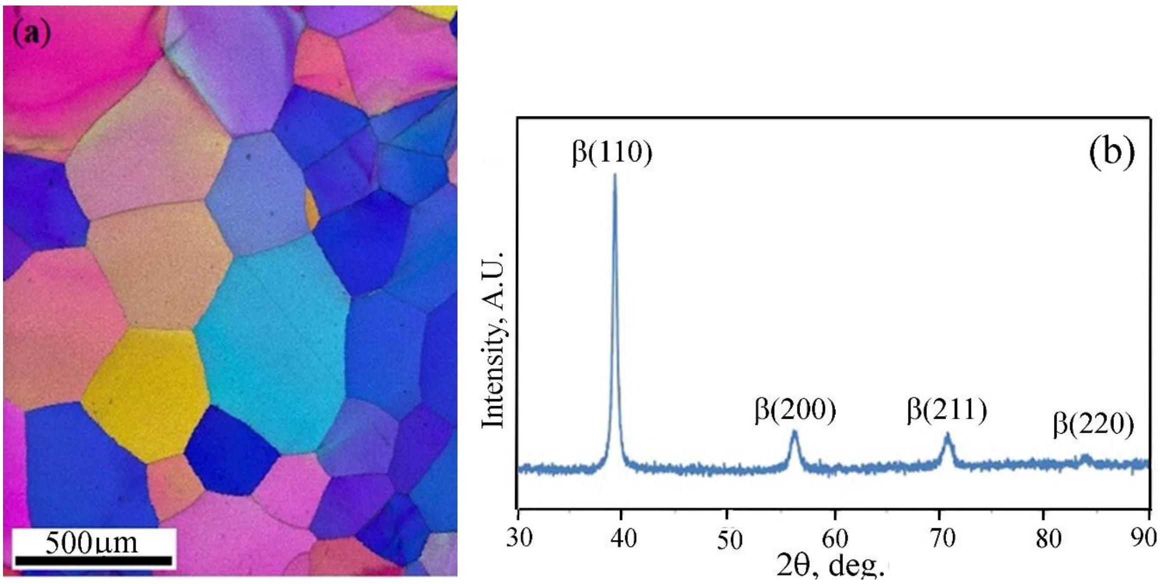

Fig. 1: (a) EBSD-IPF (inverse pole figure) map, and (b) XRD pattern of the Ti-17Mo alloy solution-treated at 1173 K for 1.8 ks.

3.2 Hot deformation behavior

The flow stress curves of the Ti-17Mo alloy acquired by compression tests at elevated temperatures are illustrated in Fig. 2. It is observed that the flow stress gradually decreases with moving the deformation strain to 0.6 at all temperatures and various strain rates. Hence, broad peak stress is apparent within the flow curves, denoting that dynamic recrystallization (DRX) operates at strain rates less than 1 s^{-1} and a high temperature of 1273 K. The peak stresses at 1273 K are diverse being 55 and 95 MPa, at the strains of 0.06 and 0.1 and strain rates 0.01 and 0.1 s^{-1}, respectively. However, the peak stress can barely be distinguished at 1 s^{-1} strain rate and high-temperatures. The flow softening at the higher strain rate of 10 s^{-1}, especially at the lowest temperature 1123 K, can be a sign of an adiabatic temperature increase during the deformation. However, the flow stress of the studied alloy is not high. This softening behavior at the high strain rate of 10 s^{-1} is attributed to the adiabatic heating generated at the high strain rate. This softening at the high strain rate was observed during the hot deformation of steel by Hamada et al [29].

It is well recognized that DRV is the principal restoration mechanism during the hot deformation of bcc structure materials due to the high diffusivity and fast dislocation annihilation arrangement. For instance, in our previous work concerning the hot deformation of β-bcc Ti-10 wt% Mn [13], we observed that dynamic recovery (DRV) works simultaneously with continuous dynamic recrystallization (CDRX). In previous studies, DRV was the main restoration mechanism on the hot deformation process of titanium alloys within the β field, due to the high SFE and the high diffusivity in the β phase-field [30, 31]. However, DRX, which is generally detected in low SFE alloys, also has been proved to occur under specific deformation conditions [32, 33]. Abbasi reported that DRV is the dominant softening mechanism for titanium Alloy (Ti-13V-11Cr-3Al β) at low strain rates with a small contribution of DRX [12]. Fan et al. [34] reported the occurrence of both DRV and DRX during hot deformation of Ti-7333 near beta titanium alloy. They found that the dynamic recrystallization degree is considerately reliant on strain rate as well as deformation temperature.

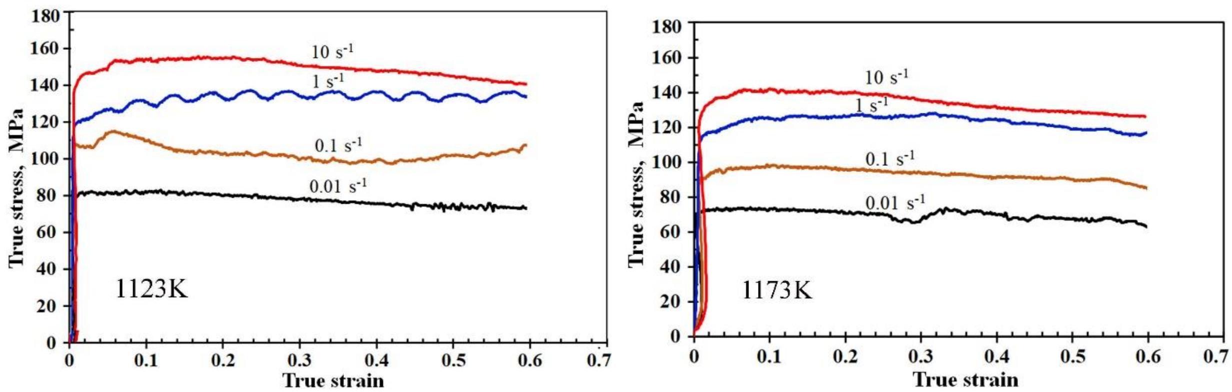

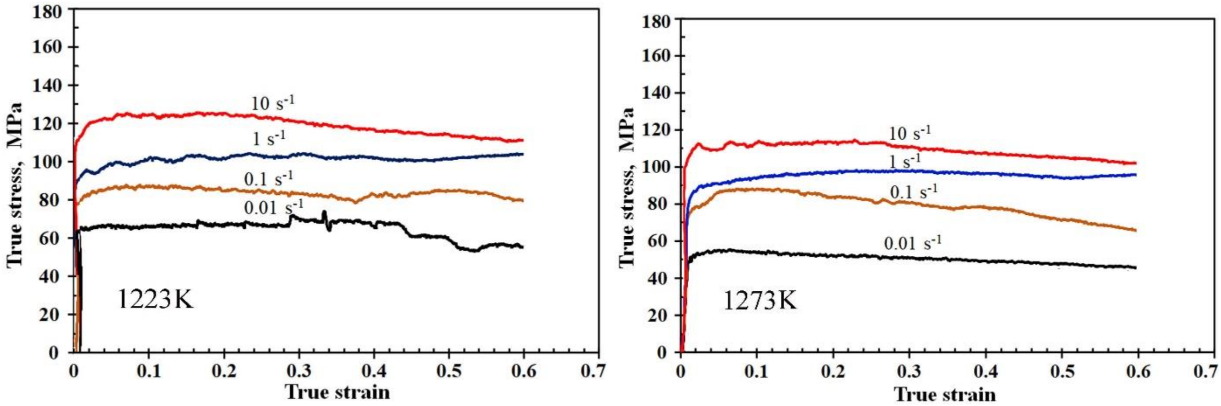

Fig. 2: Typical compressive true stress–true strain curves of Ti-17Mo alloy obtained under various strain rates in the range 0.01–10 s^{-1} and temperatures range 1123 – 1273 K.

3.3 Constitutive analysis

It is well established that, during the hot deformation the steady-state flow stress is related to temperature and strain rate throughout an Arrhenius-type of rate equation [35]. Consistent with the collected data of the hot deformation, three forms of constitutive equations (i.e., power, exponential, and hyperbolic) can be used to describe the interaction between the strain rate and temperature as follows:

The exponent-type equation for low-stress levels ($\alpha\sigma$ <0.8):

$$\dot{\varepsilon} = A\sigma^{n'}\exp\left(-\frac{Q_{HD}}{R{\cdot}T}\right) \tag{1}$$

The power exponent-type equation for high-stress levels ($\alpha\sigma$ >1.2):

$$\dot{\varepsilon} = A.\exp(\beta\sigma)\,.\,exp\left(-\frac{Q_{HD}}{R{\cdot}T}\right) \tag{2}$$

Hyperbolic sine law for all stress level:

$$\dot{\varepsilon} = A\,[sinh(\alpha\sigma)]^{n}\ \exp\left(-\frac{Q_{HD}}{R{\cdot}T}\right) \tag{3}$$

wherever σ presents the steady-state flow stress, $\dot{\varepsilon}$ presents the strain-rate, T stands for the absolute temperature; Q_{HD} represents the apparent activation energy of hot deformation; while n is stress exponent, whilst α is the stress multiplier, and R is the general gas constant (8.314 J/K mol) also A, n' and β are material factors.

For the hyperbolic sine law equation, Sellars and McTegar showed that this equation can precisely describe the constitutive behaviors of the hot deformed materials in a broad range of stress levels [36].

Material constants β and n′ can be determined by obtaining the natural logarithm on the two sections of Eqns. (1) and (2). These equations can then be re-written as Eqns. (4) and (5), respectively:

$$ln(\dot{\varepsilon}) = \ln(A) + n'\,ln(\sigma) - \frac{Q_{HD}}{RT} \tag{4}$$

$$ln(\dot{\varepsilon}) = \beta\sigma + lnA - \frac{Q_{HD}}{RT} \tag{5}$$

From Eq. (4), the material constant n′ can be determined from the graphs of ln ($\dot{\varepsilon}$) versus ln (σ) at constant temperature, Eq. (6):

$$n' = \frac{\partial \, ln(\dot{\varepsilon})}{\partial \, ln(\sigma)}\bigg|_T \tag{6}$$

Likewise, From Eq. (5), the material constant β can be estimated by plotting the relation between ln ($\dot{\varepsilon}$) and (σ) at a constant temperature, Eq. (7):

$$\beta = \frac{\partial \ln(\dot{\varepsilon})}{\partial(\sigma)}\bigg|_T \tag{7}$$

The stress multiplier parameter (α) can be calculated approximately according to the relation between β and n′ given in Eq. (8)[36]:

$$\alpha \approx \beta / n' \tag{8}$$

Thus, the n' constant value of the present Ti-17Mo alloy is obtained from ln (σ) against ln ($\dot{\varepsilon}$) plot slope and β is found from the slope of the (σ) against ln ($\dot{\varepsilon}$) plot, as shown in Fig. 3(a) and Fig. 3(b).

The linear fits show good quality fitting with the data points with an average value n' = 10.2 and the correlation coefficient is found to be ~0.97. In the same way, the β constant of the Ti-17Mo alloy is calculated from Fig. 3(b) with an average value of 0.104. Therefore, the stress multiplier (α) is anticipated to be α = β/ n' = 0.01052 for the hot deformation process of the present Ti-17Mo alloy.

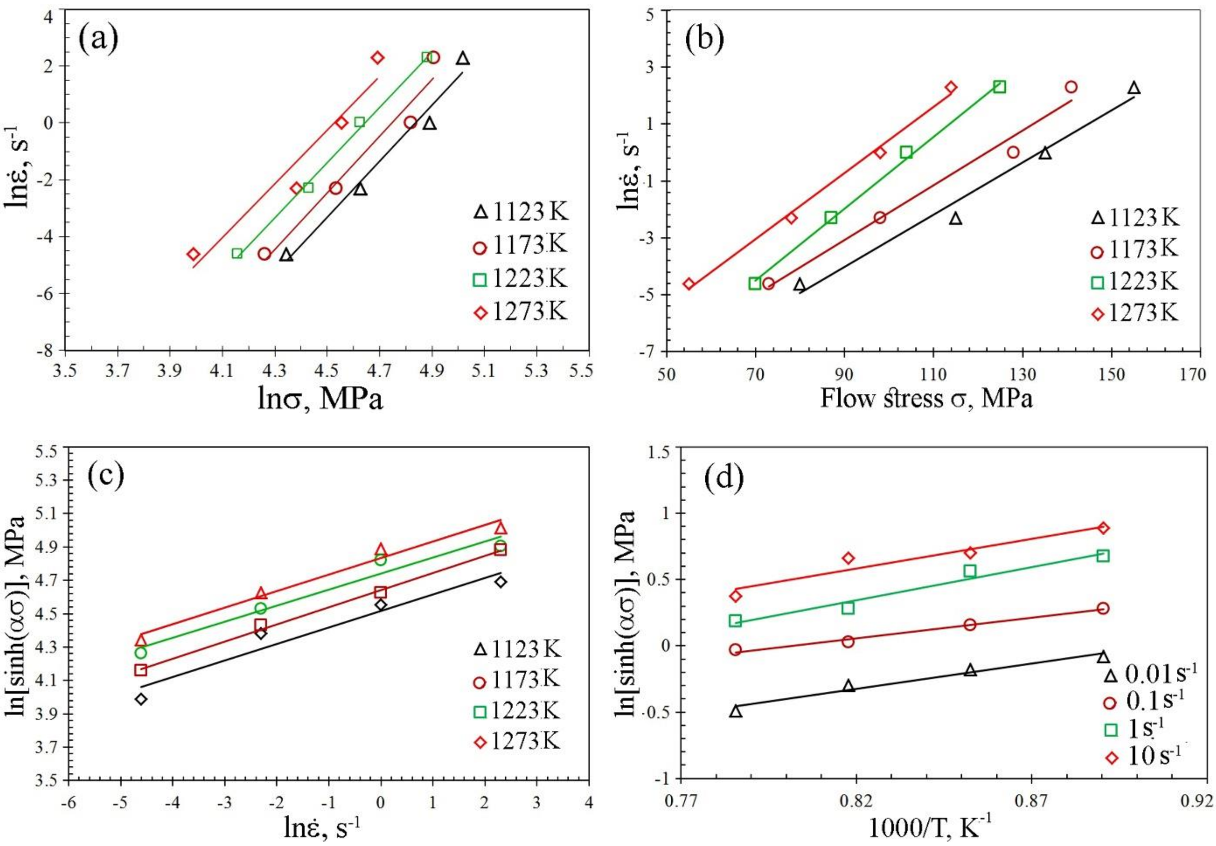

Fig. 3: The linear relationships utilized to estimate n' and β parameters at various strain rates and deformation temperatures. (a) $ln\sigma$ vs $ln\dot{\varepsilon}$, and (b) σ vs $ln\dot{\varepsilon}$. Linear regressions: (c) strain rate

dependence of ln[sinh(ασ)] to calculate the stress exponent *n*, and (d) temperature dependence of ln[sinh(ασ)] to calculate the activation energy of hot deformation.

The stress exponent value, *n*, in addition to the activation energy of hot deformation, Q_{HD}, are determined based on the hyperbolic sine law after getting the natural logarithm of both sections of Eq. 3, as illustrated in Eq. 9.

$$ln(\dot{\varepsilon}) = nln[sinh(\alpha\sigma)] + lnA - \frac{Q_{HD}}{R}\left(\frac{1}{T}\right) \quad (9)$$

The stress exponent *n* value is calculated from the slope of the drawing between $ln[\ sinh(\alpha\sigma)]$ and $ln\ (\dot{\varepsilon}\ )$ at various temperatures, as shown in Fig. 3(d).

$$n = \left.\frac{\partial\ ln(\dot{\varepsilon}\ )}{\partial\ ln[sinh(\alpha\sigma)]}\right|_T \quad (10)$$

The average result determined for the stress exponent, n of the present Ti-17Mo alloy is 8.04. It is well established that in the hot deformation process at a constant strain rate, the deformation temperature has a significant effect on the flow stress, as illustrated in Fig. 3(c). The apparent activation energy of the hot deformation can be estimated from Eq. (11):

$$Q_{HD} = R\ \left[\frac{\partial \ln \dot{\varepsilon}}{\partial \ln[\ \sinh(\alpha\sigma)]}\right]_T \left[\frac{\partial\ \ln[\ \sinh(\alpha\sigma)]}{\partial(1\ /T)}\right]_{\dot{\varepsilon}} \quad (11)$$

Fig. 3(c) shows the plot between ln $(\sinh\ (\alpha\sigma)$ and both ln $(\dot{\varepsilon})$ for various temperatures while Fig. 3(d) shows the plot relating ln$(\sinh\ (\alpha\sigma)$ and 1/T for different strain rates. Therefore, the predictive value of the average activation energy (Q) of the Ti-17Mo alloy is calculated to be approximately 283.7 kJ/mol which is a high value compared to the other known β-titanium alloys [13]. The activation energy of the hot deformation process is a substantial physical property that gives an indication of the level of difficulty during hot plastic deformation. It is well established that Mo has low diffusivity in β-titanium which elucidates the high magnitude activation energy (283.7 kJ/mol) of the hot deformation for the present alloy [37]. The average hot deformation activation energy of Ti-17Mo alloy is high compared to pure Titanium, i.e., self-diffusion activation energy, and many β-type Ti-alloys with various compositions [38-40]. This confirms that the basic restoration mechanism of β Ti-17Mo alloy is governed by DRV and CDRX at higher temperatures.

For a simple illustration, the steady state flow stress, σ, can similarly be represented by the power law function of the Zener–Hollomon parameter, Z [41, 42].

$$Z = Asinh[(\alpha\sigma)]^n \quad (12)$$

Since α and A are the material factors while *n* presents the stress exponent. It is well established that the Z parameter, $Z = \dot{\varepsilon}\ \exp\ (Q_{HD}/RT)$, combines not only the sequel of deformation temperature, but also the strain rate effect on the hot deformation performance of the material. The aforementioned values of activation energy, strain rates, and flow stresses were used in calculating the temperature compensated strain rate factor or Zener– Hollomon parameter. The logarithmic style of which is expressed as:

$$\ln(Z) = \ln A + \mathrm{n} \ln [\sinh(\alpha\sigma)] \quad (13)$$

Where ln A is the intersection of ln [sin h(ασ)]-ln (Z) line with Y-axis. Via applying the least square method, ln (Z) is plotted versus ln [sinh(ασ)]. The plot in Fig. 4 gives acceptable linear correlations involving the flow stress and Z value. Furthermore, the regression coefficient R^2 was 0.98 as shown in Fig. 4. The *n* value is calculated from the slope of the linear relation in Fig. 4. The *n* value of Ti-17Mo alloy was calculated again here and found to be 7.95. This value is almost the same as the calculated value from Fig. 3(c), which means that the application of kinetic assessment of Ti-17Mo alloy in the hot deformation process has been recognized.

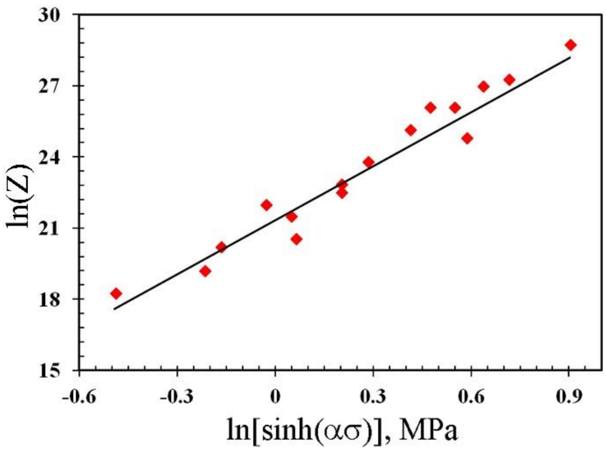

Fig. 4: Linear dependence of ln(sinh(ασ)) on ln (Z)

The material constant, A, can be computed for the present Ti-17Mo alloy from Fig. 4 and was equal to $3.4 * 10^9$. Moreover, the function representing steady-state flow stress, σ, and Zener-Hollomon parameter, *Z*, of Ti-17Mo alloy is to be presented with correlation coefficient reaches 0.98 as follow:

$$Z = 3.4 * 10^9 sinh[(0.01052\sigma)]^8 \quad (14)$$

Also, the flow stress for the Ti-17Mo titanium alloy in relation to the strain rate can be represented by a hyperbolic-sine-type equation stated as follow:

$$\dot{\varepsilon} = 3.4 * 10^9 [sinh(0.01052\sigma)]^8 \exp\left(\frac{283000}{RT}\right) \quad (15)$$

For Ti-17Mo alloy, the flow stress (σ) dependence on the strain rate ($\dot{\varepsilon}$) can be anticipated utilizing the constitutive Eq. (15).

"The experimental peak stresses and the corresponding predicted peak stresses calculated using the deduced constitutive relation in Eq. (15) are compared. Fig. 5 shows an accurate prediction of the flow stress at hot deformation of the Ti-17Mo alloy."

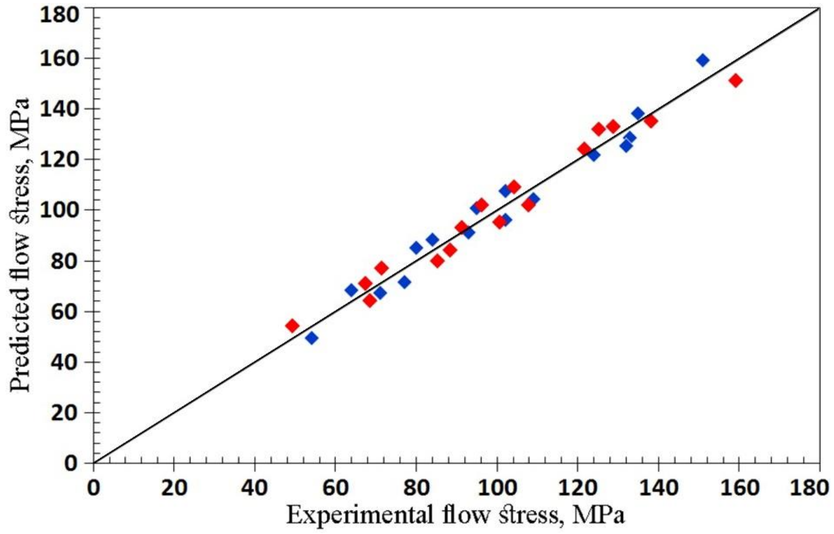

Fig. 5. Comparisons of experimental peak stresses and predicted peak stresses using the constitutive relation in Eq. (15) of the studied Ti-17Mo alloy.

3.4 Microstructural evolution of hot deformed samples

Fig. 6 shows common microstructures of β Ti-17Mo alloy after hot deformation at a temperature of 1173 K and strain rate of 0.01 s^{-1} to a true strain of about 0.6. The deformed grains are elongated perpendicular to the compression axis. At this low strain rate, the grain boundaries developed serrations at 0.6 true strain as illustrated in Fig. 6(a). The wavelength of the serrations is similar to the subgrain size. New fine recrystallized grains emerge at the serrated grain boundaries, as pointed out by the black arrows in Fig. 6(a). The EBSD-IPF map displays small fine equiaxed subgrains besides the original grain boundaries, as shown in Fig. 6(b). Few new recrystallized grains were formed, as indicated by red arrows in Fig. 6(a). Fig. 6(c) shows the relative occurrences of low-angle (green; 2–15°) and high-angle boundaries (black; >15°) seen in the microstructure in Fig. 6(b) are plotted in Fig. 6(c). The fraction of low-angle boundaries is high (about 0.7), indicating few fully recrystallized grains are formed with HAGBs, which indicates that dynamic recovery (DRV) is the dominant softening mechanism at a low strain rate of 0.01s^{-1}. However, there is a peak at a misorientation angle of less than 30° which can be related to the new small recrystallized grains, resulting from the DDRX process [12]. In agreement with Fan et al. [21], the hot deformation behavior of the β-Ti alloys is mainly dominated by the softening mechanism DRV at elevated temperatures and low strain rates (e.g., 0.01 s^{-1}). They claimed that the DRV activated at high temperature deformation with low strain rates is directly connected to the lattice diffusion.

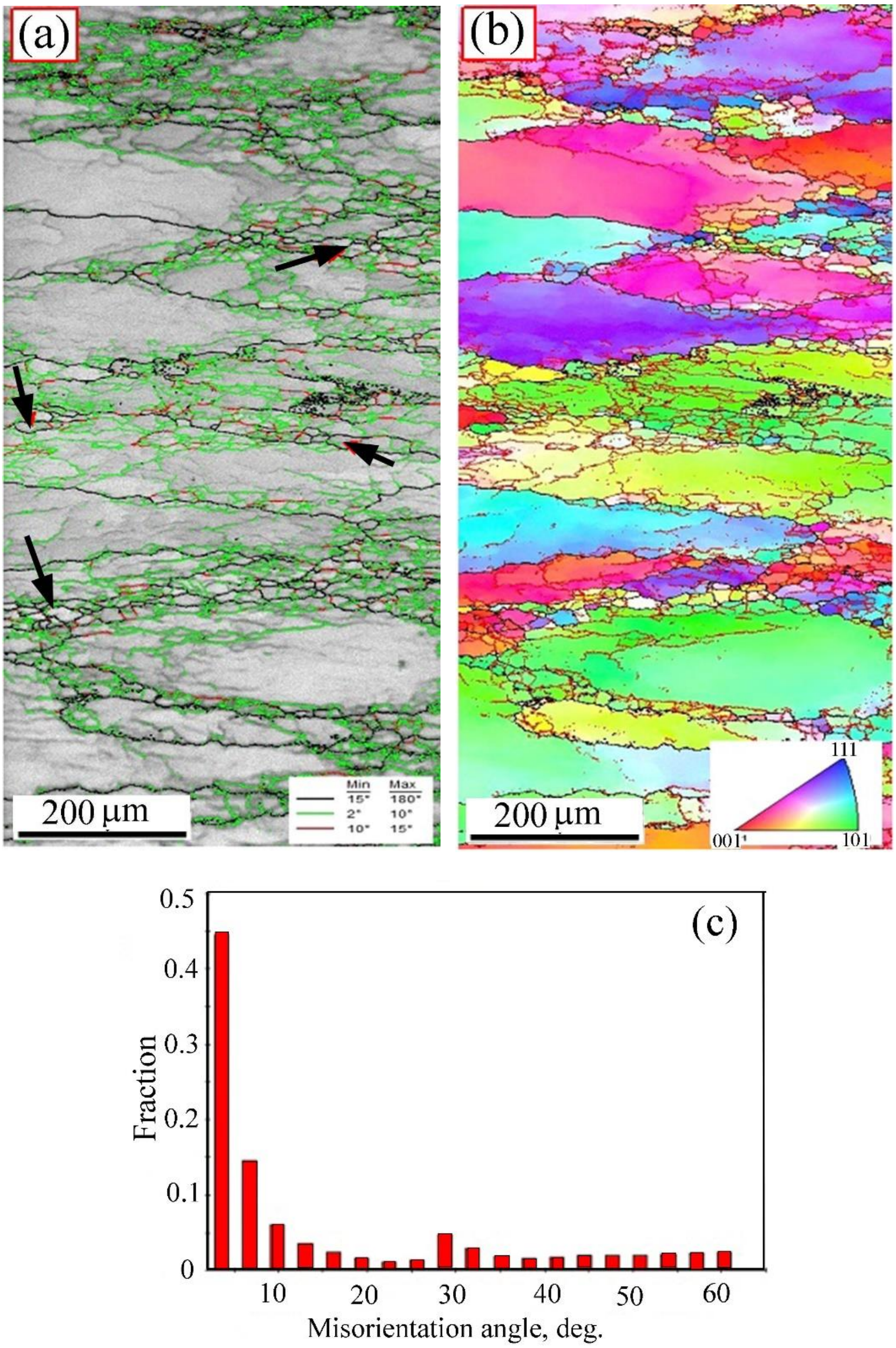

Fig. 6: Microstructure of Ti-17Mo alloy hot worked to 0.6 true strain at 1173 K/ 0.01 s^{-1}. (a) EBSD-boundary map (b) Misorientation map (low-angle boundaries shown in red color) (c) Relative fraction of LAGBs and HAGBs corresponding to (b).

However, with the deformation temperature being raised to 1273 K at a similar strain rate of 0.01s^{-1}, the DDRX process is activated further, and the microstructure undergoes large equiaxed grains along the grains boundaries and specifically at the triple points, as shown in Fig. 7(a).

Along with this, some un-recrystallized elongated grains are still observed. The recrystallized grains become coarser compared to a lower temperature (i.e., 1173 K), as shown in Fig. 6(b). The coarsening process of the recrystallized grain can be linked with the increase in the deformation temperature that supports the diffusion process for new grains growth [43]. Sub-structures are still detected in the initial large, pancaked grains, as shown in Fig. 7(c). The low-misorientation boundaries ratio, i.e., sub-grains boundaries, of the hot-deformed structure of Fig. 7(a), is nearly 0.57, as represented in Fig. 7(d). Again, the many sub-grain boundaries apparent, indicate active DRV through the hot deformation process of β Ti-17Mo alloy at a low strain rate of 0.01 s^{-1} and 1273 K, yet with less amount compared to 1173 K. In contrast, the formation of new grains by DDRX was induced in the deformed structure, as indicated in Fig. 7(b).

The microstructure of Ti-17Mo alloy hot-deformed at 1173 K and strain rate of 10 s^{-1} is displayed in Fig. 8(a). By increasing the strain rate, the grain boundaries converted to be straight boundaries. A new morphology of the deformed grain appears in the form of fine ribbon grains indicated by the black arrows in Fig. 8(b).

Furthermore, few HAGBs are initiated in the original deformed grain interior as pointed out by white arrows in Fig. 8(b). These HAGBs look like deformation banding induced boundaries promoted at such a high strain rate. Also, the grain rotation and distortion, as indicated by the color gradient in Fig. 8(b), are clearly observed in some coarse grains at such high strain rates. This retained grains distortion after deformation at 1173 K is most probably related to the applied high strain rate that did not allow full-grain recovery or recrystallization.

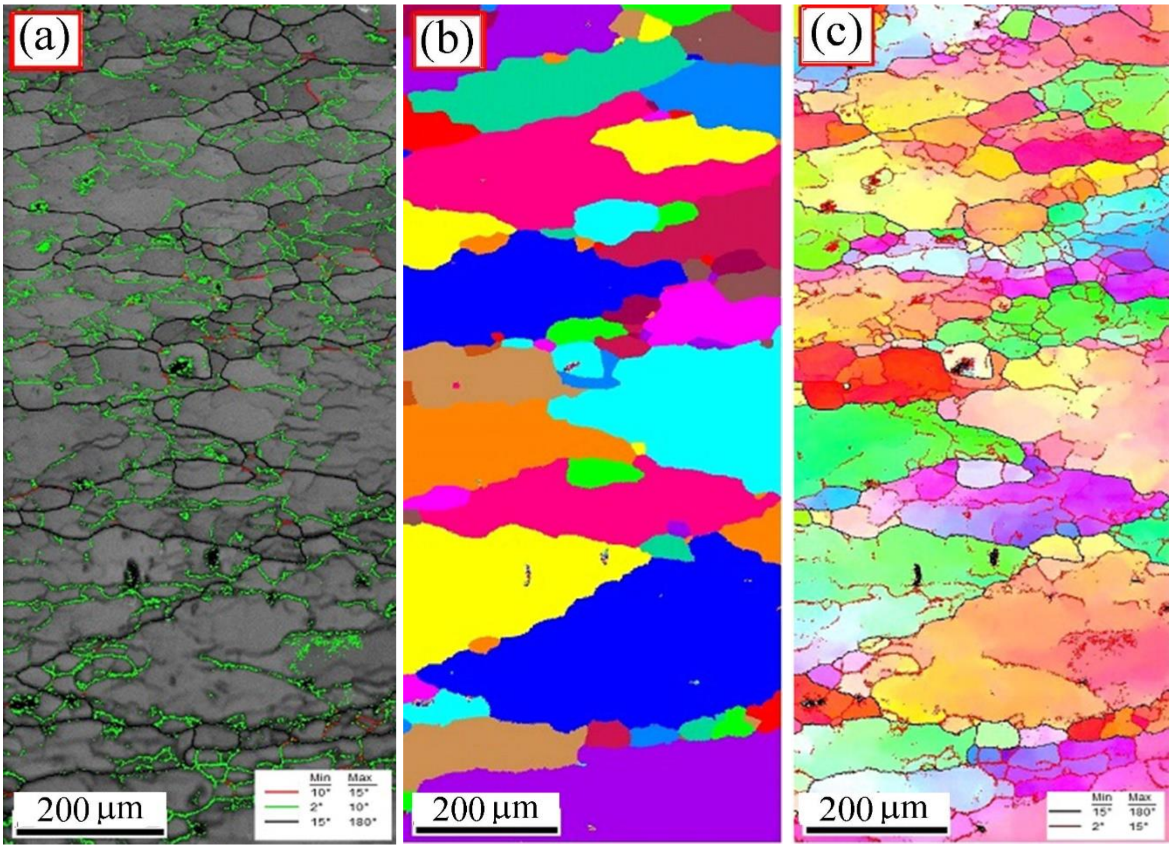

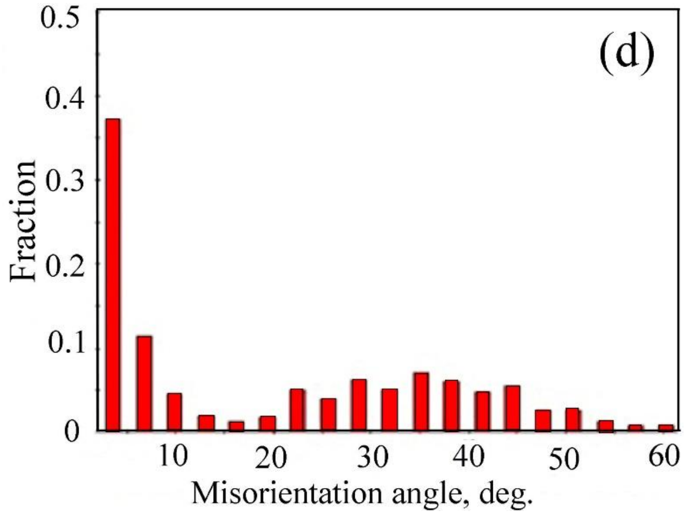

Fig. 7: Microstructure of Ti-17Mo alloy hot worked to 0.6 true strain at 1273 K/ 0.01 s^{-1}: (a) EBSD-Boundary map, (b) quick colored map, and (c)Misorientation map. (d)) Relative fraction of LAGBs and HAGBs corresponding to (c).

Kuhlmann et al. [22] reported that the development of DBs (deformation bands) is usually related to the selection process of the effective slip systems in the grain interior to reduce the energy consumption during the deformation process, especially for coarse-grained material. If the applied strain is distributed non-uniformly inside the deformed specimen the generation of DB can be promoted [44, 45]. The boundaries of the deformation bands are sharp, which are like the HAGBs. These sharp boundaries will hinder the recrystallization process.

The relative fractions of the low-angle boundaries (green and red lines; 2–15°), as well as the high-angle boundaries (black lines; >15°) appearing in the microstructure (Fig. 8(a)), are plotted in Fig. 8(c). At such conditions, low angle grain boundaries presence is rather high. This proves that the predominant softening mechanism during the hot deformation of the studied alloy at1173 K and 10 s^{-1} is DRV.

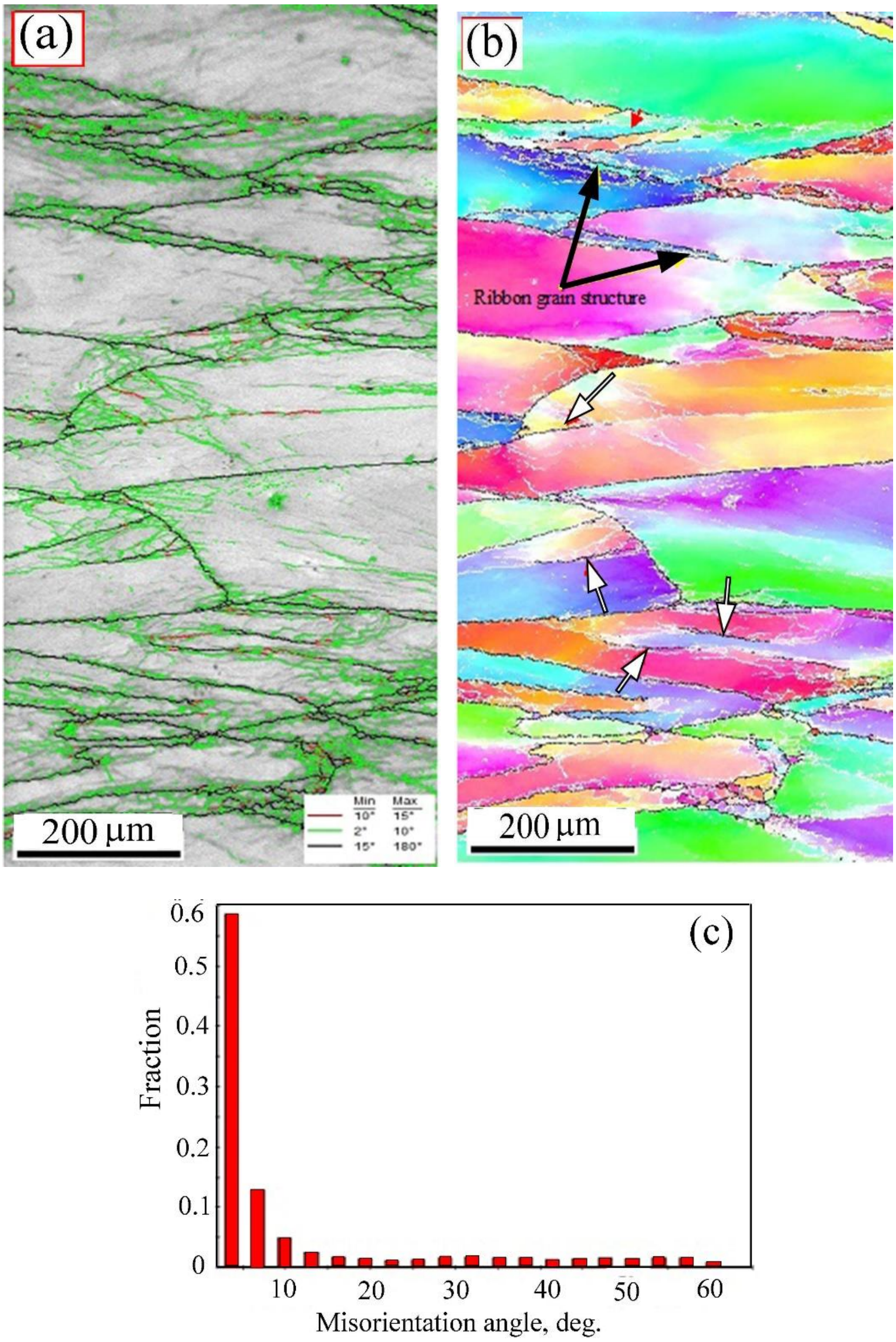

Fig. 8: EBSD maps of the microstructure of Ti-17Mo alloy hot worked to 0.6 true strain at 1173 K/ 10 s^{-1}: (a) EBSD-boundary map, (b) EBSD +IPF map, (c) Relative fraction of LAGBs and HAGBs corresponding to (a).

However, with increasing the deformation temperature to 1273 K at the high strain rate 10 s^{-1}, new fine recrystallized grains are formed alongside the grain boundaries and within the parent grains due to CDRX, as shown in colored coded map Fig. 9(b). Fig. 9(d) shows the relative fractions of the low-angle (green and red lines; 2–15°) and the high-angle boundaries (black lines >15°) seen in the microstructure (Fig. 9(a)). Furthermore, the fraction of the low-angle (<15°) boundaries is almost the same as at 1173 K /10 s^{-1}, see Fig. 8(d).

Intensive observations of the microstructural features in the current work demonstrated the hot deformation process of Ti-17Mo alloy displays a propensity to DDRX with increasing the deformation temperature and lowering strain rate. At the high temperature 1273 K and a low strain rate of 0.01 s^{-1} both the DRV and DDRX were active restoration mechanisms. This can also be observed in the flow curve at 1273 K/ 0.01 s^{-1}, which shows softening behavior as a result of the DDRX process.

However, at the high strain rate DRV was the predominant deformation mechanism with a small amount of CDRX behavior which can be linked also with the flow curve in both conditions because the flow curves at high strain rate 10 s^{-1} and temperatures 1173-1273 K show almost plateau up to 0.3 strain and then very small softening which can be related to the slight effect of the adiabatic heating at high strain rate not to the DRX process.

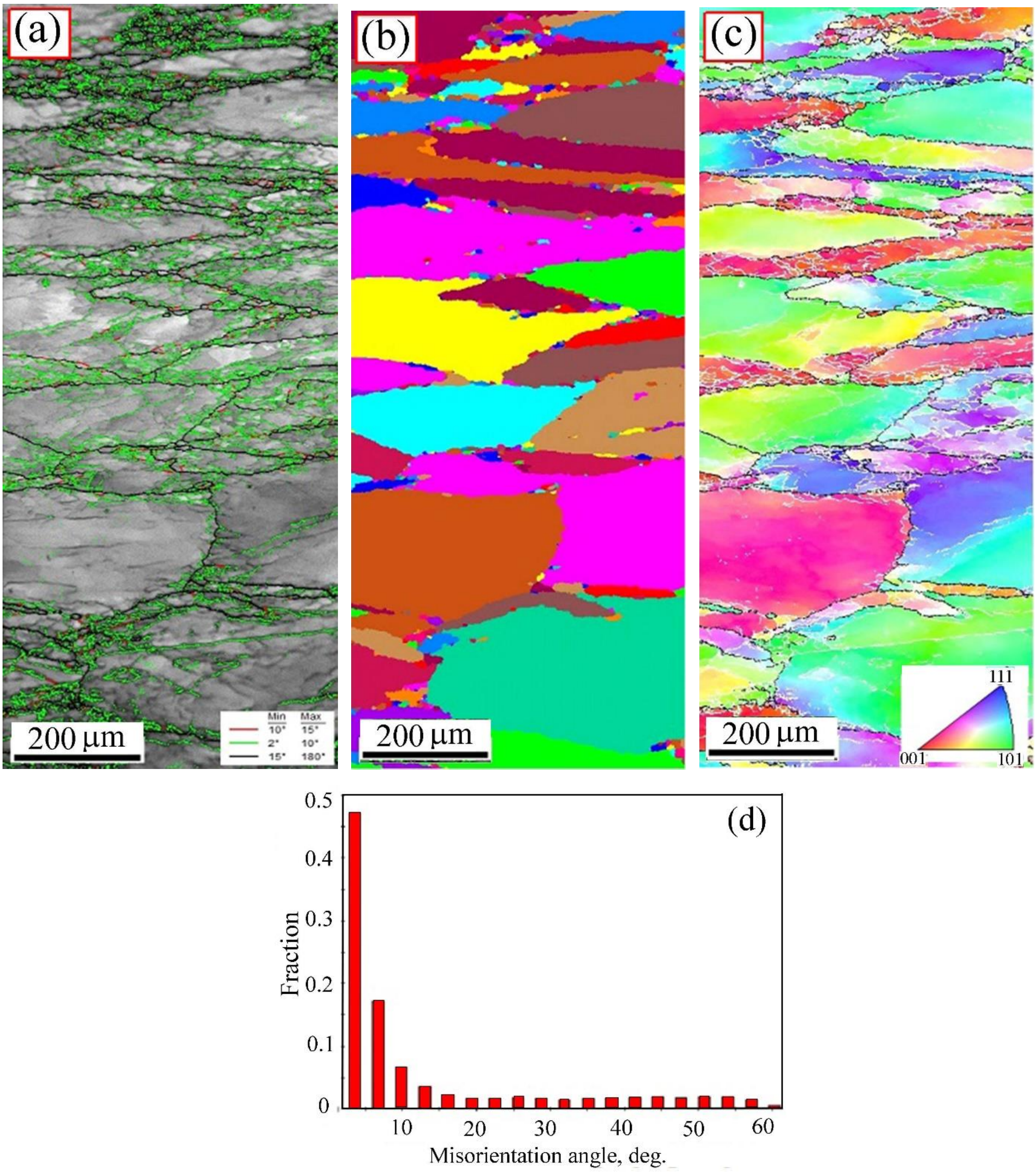

Fig. 9: EBSD maps of Ti-17Mo alloy microstructure hot worked to 0.6 true strain at 1273 K /10 s^{-1}. (a) EBSD-boundary map (b) Quick colored map (c) Misorientation map, (d) Relative fractions of LAGBs and HAGBs corresponding to (b).

On the other hand, at the high strain rate of 10 s^{-1} deformation banding is enhanced. Moreover, the microstructural observations revealed that the hot deformation of the Ti-17Mo alloy at high strain rates (10 s^{-1}) is more sensitive to temperature. This finding is in agreement with the work of Balasubrahmanyam and Prasad [46] who observed that the hot deformation behavior of the Ti–10V–4.5Fe–1.5Al beta alloy depends on the deformation temperature at a high strain rate.

Conclusions:

In this study, the microstructural development and the flow behavior of β-type Ti-17Mo alloy were investigated through hot compressions tests at temperatures in the range of 1123 K – 1273 K at a strain rate range of 0.01 – 10 s^{-1}. The major results can be summed up as follows:

1. The hot deformation parameters have a substantial effect on microstructure development. Elevating the deformation temperature and reducing the strain rate support the DRX process. In the present deformation conditions, the dominant working mechanism is concurrent DRV and DRX at a deformation temperature of 1273 K.
2. The microstructural examination showed that DRV was more prevalent than DRX as a softening mechanism at every deformation temperature and especially at lower strain rates.
3. The initial coarse structure induces DBs as an additional deformation mechanism, which suppresses the DRX process, at a high strain rate.
4. The activation energy of hot working for Ti-17Mo alloy in the β- field is 283 kJ/mol according to calculations, which is a relatively high value compared to most known β-type Ti-alloys.
5 .Based on the hot deformation study of the Ti-17Mo alloy, a correlation amongst strain rate, temperature, and flow stress were deduced as:

$$\dot{\varepsilon} = 3.4*10^{9}\,[\sinh(0.01052\sigma)]^{8}\exp^{(283,000/RT)}$$

Acknowledgments:

The authors thankfully acknowledge the financial support from the Missions Sector-Higher Education Ministry, Egypt, and the Japan International Cooperation Agency (JICA) through this work. This work is in the frame of the joint research project ASRT/DST research project.

Data availability:

The raw/processed data required to reproduce these findings cannot be shared at this time due to technical or time limitations.

Conflict of interest

On behalf of all authors, the corresponding author states that there is no conflict of interest.

References

1. M. J. Donachie, *Titanium a Technical Guide*, 2nd ed. (ASM International, 2000).

2. J. C. Lütjering, Gerd, Williams, *Titanium* (Springer, 2007).

3. F. Geng, M. Niinomi, and M. Nakai, Mater. Sci. Eng. A **528**, 5435 (2011).

4. O. P. Karasevskaya, O. M. Ivasishin, S. L. Semiatin, and Y. V. Matviychuk, Mater. Sci. Eng. A **354**, 121 (2003).

5. H. Matsumoto, S. Watanabe, and S. Hanada, J. Alloys Compd. **439**, 146 (2007).

6. H. Liu, M. Niinomi, M. Nakai, and K. Cho, ACTA Biomater. **24**, 361 (2015).

7. L. Zardiackas, D. Mitchell, and J. Disegi, "Characterization of Ti-15Mo Beta Titanium Alloy for Orthopaedic Implant Applications," in *Medical Applications of Titanium and Its Alloys: The Material and Biological Issues*, ed. S. Brown and J. Lemons (West Conshohocken, PA: ASTM International, 1996), 60-75. https://doi.org/10.1520/STP16070S

8. X. Zhao, M. Niinomi, M. Nakai, and J. Hieda, **8**, Acta Biomater.1990 (2012).

9. J. K. Fan, H. C. Kou, M. J. Lai, B. Tang, H. Chang, and J. S. Li, Mater. Sci. Eng. A **584**, 121 (2013).

10. S. M. Abbasi, A. Momeni, Y. C. Lin, and H. R. Jafarian, Mater. Sci. Eng. A **665**, 154 (2016).

11. X.-Q. Yin, C.-H. Park, Y.-F. Li, W.-J. Ye, Y.-T. Zuo, S.-W. Lee, J.-T. Yeom, and X.-J. Mi, J. Alloys Compd. **693**, 426 (2017).

12. S. M. Abbasi, M. Morakkabati, A. H. Sheikhali, and A. Momeni, Metall. Mater. Trans. A Phys. Metall. Mater. Sci. **45**, 5201 (2014).

13. S. Ebied, A. Hamada, W. Borek, M. Gepreel, and A. Chiba, Mater. Charact. **139**, 176 (2018).

14. F. Montheillet, L. Pallot, and D. Piot, Mater. Sci. Forum **706–709**, 127 (2012).

15. S. M. Abbasi, A. Momeni, A. Akhondzadeh, and S. M. Ghazi Mirsaed, Mater. Sci. Eng. A **639**, 21 (2015).

16. A. Momeni and S. M. Abbasi, Mater. Des. **31**, 3599 (2010).

17. H. Matsumoto, L. Bin, S. H. Lee, Y. Li, Y. Ono, and A. Chiba, Metall. Mater. Trans. A Phys. Metall. Mater. Sci. **44**, 3245 (2013).

18. T. Furuhara, Y. Toji, H. Abe, and T. Maki, Mater. Sci. Forum **426–432**, 655 (2003).

19. C. R. H. Darren G. Cram, Hatem S. Zurob, Yves J.M. Bréchet, Mater. Sci. Forum **715–716**, 492 (2012).

20. A. H. Sheikhali, M. Morakkabati, S. M. Abbasi, and A. Rezaei, Int. J. Mater. Res. **104**, 3 (2013).

21. X. G. Fan, Y. Zhang, P. F. Gao, Z. N. Lei, and M. Zhan, Mater. Sci. Eng. A **694**, 24 (2017).

22. D. Kuhlmann-Wilsdorf, Acta Mater. **47**, 1697 (1999).

23. X. G. Fan, Y. Zhang, H. J. Zheng, Z. Q. Zhang, P. F. Gao, and M. Zhan, Mater. Charact. **137**, 151

(2018).
24. P. Li, X. Ma, T. Tong, and Y. Wang, J. Alloys Compd. **815**, 152412 (2020).
25. W. Xu, M. Chen, X. Lu, D. wei Zhang, H. preet Singh, Y. Jian-shu, Y. Pan, X. hui Qu, and C. zong Liu, Corros. Sci. **168**, 108557 (2020).
26. M. Fellah, N. Hezil, M. Abdul Samad, R. Djellabi, A. Montagne, A. Mejias, S. Kossman, A. Iost, A. Purnama, A. Obrosov, and S. Weiss, J. Mater. Eng. Perform. **28**, 5988 (2019).
27. K. D. Ralston, D. Fabijanic, and N. Birbilis, Electrochim. Acta **56**, 1729 (2011).
28. S. M. Ebied, M. A.-H. Gepreel, and A. Hamada, IOP Conf. Ser. Mater. Sci. Eng. **201**, 012047 (2017).
29. A. Hamada, T. Juuti, A. Khosravifard, A. Kisko, P. Karjalainen, D. Porter, and J. Kömi, Mater. Des. **154**, 117 (2018).
30. J. Zhang, H. Di, H. Wang, K. Mao, T. Ma, and Y. Cao, J. Mater. Sci. **47**, 4000 (2012).
31. Y. Liu and T. N. Baker, Mater. Sci. Eng. A **197**, 125 (1995).
32. T. Furuhara, B. Poorganji, H. Abe, and T. Maki, JOM **59**, 64 (2007).
33. P. Wanjara, M. Jahazi, H. Monajati, S. Yue, and J. P. Immarigeon, Mater. Sci. Eng. A **396**, 50 (2005).
34. J. K. Fan, H. C. Kou, M. J. Lai, B. Tang, H. Chang, and J. S. Li, Mater. Des. **49**, 945 (2013).
35. J. J. Jonas, C. M. Sellars, and W. J. M. G. Tegart, Metall. Rev. **14**, 1 (1969).
36. C. M. Sellars and W. J. McTegart, Acta Metall. **14**, 1136 (1966).
37. H. Nakajima and M. Koiwa, ISIJ International **31**, 757 (1991).
38. H. Matsumoto, S. Watanabe, and S. Hanada, Mater. Trans. **46**, 1070 (2005).
39. E. Bertrand, P. Castany, I. Péron, and T. Gloriant, Scr. Mater. **64**, 1110 (2011).
40. X. Min, S. Emura, L. Zhang, K. Tsuzaki, and K. Tsuchiya, Mater. Sci. Eng. A **646**, 279 (2015).
41. X. Ma, F. Li, J. Cao, J. Li, Z. Sun, G. Zhu, and S. Zhou, Mater. Sci. Eng. A **710**, 1 (2018).
42. P. Barriobero-Vila, J. Gussone, K. Kelm, J. Haubrich, A. Stark, N. Schell, and G. Requena, Mater. Sci. Eng. A **717**, 134 (2018).
43. P. L. Mao, G. Y. Su, and K. Yang, Mater. Sci. Technol. **18**, 892, (2002).
44. S. Kingklang and V. Uthaisangsuk, Metall. Mater. Trans. A Phys. Metall. Mater. Sci. **48**, 95 (2017).
45. C. Zener and J. H. Hollomon, J. Appl. Phys. **15**, 22 (1944).
46. V. V. Balasubrahmanyam and Y. V. R. K. Prasad, Mater. Sci. Eng. A **336**, 150 (2002).